Initial experience of integrated PET/MR mammography in patients with invasive ductal carcinoma

Eun-Jung Kong[1], MD
Kyung-Ah Chun[1], MD
Hee-Seung Bom[2], MD
Jaetae Lee[3], MD
Soo-Jung Lee[4], MD
Ihn-Ho Cho[1]MD

1. Department of Nuclear Medicine, College of Medicine, Yeungnam University, Daegu, Republic of Korea
2. Department of Nuclear Medicine, College of Medicine, Chonnam National University, Gwangju, Republic of Korea
3. Department of Nuclear Medicine, Kyungpook National University, School of Medicine, Daegu, Republic of Korea
4. Department of Surgery, College of Medicine, Yeungnam University, Daegu, Republic of Korea

Keywords: Breast cancer - Invasive ductal carcinoma - MR mammography - PET/MRI - Hybrid imaging

Correspondence address:
Ihn Ho Cho,
317-1 Daemyeong 5-dong,
Nam-gu, Daegu 705-717,
Korea
Tel: +82-53-620-3074,
Fax: +82-53-620-3079
E-mail: ihcho@med.yu.ac.kr

Received:
18 August 2014
Accepted revised:
29 August 2014

Abstract

The purpose of this study was to evaluate the feasibility of integrated fluorine-18-fluorodeoxyglucose positron emission tomography/magnetic resonance (^{18}F-FDG PET/MR) mammography in invasive ductal carcinoma (IDC) patients. *From August 2012 to March 2013, we enrolled* 42 consecutive breast cancer patients who received whole- body PET/MR and subsequent PET/MR mammography by an integrated PET/MR scanner and were scheduled for surgery within 2 weeks after the of scan. On the whole body PET/MR, 2-point Dixon VIBE, coronal T1w image, axial T2w image, and post-contrast T1 sequences were acquired with simultaneous PET acquisition. For PET/MR mammography, T1w, T2w, and dynamic contrast-enhancement (DCE) sequences were acquired using a breast coil during simultaneous PET acquisition. We compared the detectability of the lesions between whole-body PET/MR and PET/MR mammography. *Forty-eight* IDC (1.89±1.19cm of width) were diagnosed in 42 women. Lesion conspicuity in ^{18}F-FDG PET was equivalent between whole-body PET/MR and PET/MR mammography; both PET/MR images showed 38 hypermetabolic masses. In the analysis of 10 IDC with <1.0cm wide lesions, only 1 IDC showed ^{18}F-FDG uptake, and 4 IDC were noted on whole-body PET/MR; however, all 10 IDC showed a depictable mass on PET/MR mammography. In the analysis of 38 IDC >1.0cm wide, 37 IDC showed ^{18}F-FDG uptake, and 38 IDC were detected on both whole-body PET/MR and PET/MR mammography. The overall sensitivity was 79.2% (38/48) on PET, 87.5% (42/48) on whole-body PET/MR, and 100% on PET/MR mammography. The SUV between whole-body PET/MR and PET/MR mammography showed strong and highly significant correlation (r=0.987, P<0.001). *In conclusion*, our results, although in a limited number of cases showed that integrated PET/MR mammography is feasible and has the advantage of combining high-resolution breast images with metabolic images. Furthermore, PET/MR mammography could provide an accurate diagnosis of IDC that are less than 1cm in size.

Hell J Nucl Med 2014; 17(3): 171-176 *Epub ahead of print: 12 November 2014* *Published online: 22 December 2014*

Introduction

The success of hybrid imaging using positron emission tomography (PET) and computed tomography (CT) has inspired physicians and medical physicists to develop a technically challenging but academically fascinating integrated imaging system-involving PET and magnetic resonance (MR) imaging. This hybrid PET/MR imaging modality is of diagnostic value when the superior features of MR are desired (e.g., in cases of increased soft tissue contrast or reduced radiation dose and functional information). Recently, an integrated PET/MR scanner became available, and several reports on the clinical evaluation of PET/MR imaging have been published. According to these initial experiences, the image quality in integrated PET/MR is equivalent to that of PET/CT and meets oncologic diagnostic needs [1-3]. However, the ongoing challenge is to make optimum use of the integrated PET/MR scanner. Accordingly, it is necessary to identify the clinical indications that warrant its use and to establish a scanning protocol in clinical practice.

Fluorine-18-fluorodeoxyglucose (^{18}F-FDG) PET has been established as an important imaging modality for the diagnosis, staging, restaging, monitoring of the response to treatment, and estimation of the long-term prognosis in patients with breast cancer [4-7]. With both whole-body PET and PET/CT, however, the accuracy of detection and quantification of breast cancer is significantly reduced when the lesion is smaller than 1cm or shows low ^{18}F-FDG avidity [8, 9]. Computed tomography is beneficial in the diagnosis of such lesions; however, PET/CT does not provide an accurate depiction of the anatomy of the breast, primarily due to the weak soft-tissue contrast on CT. On the other hand, MR imaging (MRI) with a breast coil clearly depicts the anatomy of the breast. Therefore, for the evaluation of breast cancer, it might be worthwhile to integrate PET and MRI so that the anatomical, functional, and metabolic data are analyzed together, potentially

producing synergistic effects. Thus far, an integrated PET/MR system has not been used for the evaluation of breast cancer. We believe that the field of oncology would benefit from whole-body staging of breast cancer together with high-spatial resolution imaging of the breast for surgical planning. Thus, the goal of this study was to evaluate, for the first time, the use of an integrated ^{18}F-FDG PET/MR mammography system for the detection of primary lesions in patients with invasive ductal carcinoma (IDC).

Material and methods

The protocol of this study was approved by our institutional review board. In addition, informed consent was obtained from all the patients enrolled in this study.

Patients

From August 2012 to March 2013, PET/MR examinations were performed in 312 consecutive patients for the evaluation of breast cancer at our department. After reviewing their pathological results, we had identified 48 IDC in 42 women. These 42 women were enrolled in our study. They underwent a PET/MR examination for pre-operative evaluation and subsequently received surgery within 2 weeks of the scan. The exclusion criteria were: previous excisional biopsy, neoadjuvant chemotherapy, and known distant metastases. In addition, patients with IDC containing ductal carcinoma in situ (DCIS) were excluded from this study.

Imaging protocol

Patients fasted for at least 6h before the intravenous administration of ^{18}F-FDG (mean, 270.5±65.9MBq; range, 176.1-490.6MBq). Before the injection of the radioisotope, the blood glucose concentration was confirmed below 150mg/dL. First, a supine whole-body PET/MR scan was performed 60-90min after the injection of ^{18}F-FDG, covering a field of view from the skull base to the mid thighs. After whole-body PET/MR was completed, PET/MR mammography was performed with the patients in the prone position; the scan was started approximately 90-120min after the injection. The integrated PET/MR (BiographmMR; Siemens Healthcare, Erlangen, Germany) scanner consisted of a 3-T MR system and an inline PET system with an avalanche photodiodes (APD) detector. The APD are not only insensitive to a magnetic field but also have a small space to be cased within the MR gantry. The PET unit has an axial field of view of 25.8 cm and offers the advantage of fewer bed positions in a short time. The PET data were reconstructed using a 3-dimensional (3D) ordinary Poisson ordered-subsets expectation (OP-OSEM) algorithm with 2 iterations and 21 subsets (172×172 matrix, zoom 1, slice thickness 2mm). A post-reconstruction Gaussian filter with 6.0mm full-width at half-maximum was applied. An MRI-based attenuation correction of the PET data was accomplished according to the method described by Martinez-Möller et al [10].

The imaging protocol was designed with reference to the study by Martinez-Möller et al [11]. Whole-body PET/MR was performed in a caudocranial direction, with a total imaging matrix (TIM) coil. The TIM coil is an approved surface coil for PET/MR, which improves image quality and reduces imaging time with MRI, similar to that in standalone MRI. After acquisition of the initial T1-weighted two-point Dixon 3D volumetric interpolated breath-hold examination (VIBE) for attenuation correction, coronal T1-weighted turbo spin-echo (TSE) and axial T2-weighted fat saturated (fs) half-Fourier single-shot turbo spin-echo (HASTE) sequences were obtained during simultaneous PET acquisition. Four PET bed positions were usually required, and the emission time per bed was 3min.

The PET/MR mammography comprised a breast PET scan of 1 bed position and a simultaneous breast MRI using a standard 16-channel AI Breast Coil (RAPID Biomedical GmbH, Rimpar, Germany) device. The emission time of the PET scan was 8min. The breast MRI examination consisted of a localizer sequence, T1-weighted TSE, and T2-weighted fs TSE sequence, a single-shot spin-echo planar diffusion-weighted sequence, and 3D dynamic contrast-enhanced (DCE) sequence. DCE-MRI was performed with axial T1 3D VIBE imaging, with 1 pre-contrast and 5 post-contrast dynamic series performed within 5:18–8:22 depending on the breast thickness after bolus injection. Next, 3mL/s of gadopentetated-

Table 1. *Technical parameters for different MRI sequences*

Sequence	Image plane	TE/TR(ms)	Slice thickness (mm)	Matrix/ resolution(mm^2)	GRAPPA	Protocol time
Whole-body PET/MR						
AC Dixon VIBE	coronal	1.23/3.6	3.12	172×172 / 4.10×2.60	2	0:19
T1 TSE	coronal	8.8/557	6	384×202 / 1.67×1.17	3	0:35
HASTE	axial	67/1000	4	320×180 / 1.67×1.25	2	0:54
VIBE T1w	axial	1.26/3.28	3	320×195 / 1.58×1.19	2	0:16
PET/MR mammography						
AC Dixon VIBE	coronal	1.23/3.6	3.12	172×172 / 4.10×2.60	2	0:19
T1w TSE	axial	9.8/700	3	448×358 / 0.95×0.76	3	1:20
fs T2w TSE	axial	72/5300	3	448×314 / 1.08×0.76	2	3:11
DWI	axial	86/8400	3	192×77 / 2.28×1.82	3	3:12
DCE	axial	1.48/4.07	1.2	416×333 / 1.02×0.82	3	7:21

AC: attenuation correction; CM: contrast medium; DCE: dynamic contrast enhanced; DWI: diffusion weighted imaging; fs: fat saturated; GRAPPA: generalized autocalibrating partially-parallel acquisition; HASTE: half Fourier acquisition single shot turbo spin echo; TE: echo time; TR: repetition time; TSE: turbo spin echo; VIBE: 3-dimensional volumetric interpolated breath-hold examination.

Table 2. *Acquisition protocol for whole-body PET/MR and PET/MR mammography using the integrated PET/MR scanner*

Module	Region	PET acquisition	MRI sequence	Position	Coil	Scan time
Whole body PET/MR	Skull base - thigh	Bed position PET (3min/bed)	AC cor T1 ax HASTE fs	Supine position (4 beds)	TIM coil	Start
PET/MR mammography	Breast	1 bed (8min)	AC ax T1 TSE ax T2 TSE fs axDWI ax DCE after CM	Prone position	Breast coil	30min
MR only	Lung - pelvis	No PET	ax VIBE	Supine (3 beds)	TIM coil	60-70 min

AC: attenuation correction; ax: axial; CM: contrast medium; cor: coronal; DCE: dynamic contrast enhancement; DWI: diffusion-weighted imaging; fs: fat-saturated; HASTE: half Fourier acquisition single-shot turbo spin-echo; TSE: turbo spin-echo; VIBE: 3-dimensional volumetric interpolated breath-hold examination

imeglumine (0.1mmol/kg of body weight, MRbester, Taejoon Pharm, Seoul, Republic of Korea) was injected, followed by a 20mL saline flush. Finally, in the supine position, 3-axial T1-weighted fs VIBE sequences were obtained again for the whole lung, abdomen, and pelvis, during a single breath hold, respectively. The detailed protocol used for whole-body PET/MR and PET/MR mammography using the integrated PET/MR scanner is listed in Tables 1 and 2.

Image analysis

The analysis of whole-body PET/MR and PET/MR mammography images was performed by 2 nuclear medicine physicians. The PET and MR data sets were retrospectively analyzed on the PET/MR workstation (syngo.via; Siemens Medical Solutions) by using software (mMR general and MR BreVis; Siemens Medical Solutions).

Whole-body PET/MR

The PET images were evaluated visually and quantitatively. During visual analysis, the images were classified as follows: no distinguishable uptake (G0), suspicious increased uptake (G1), mild uptake (G2), and obvious uptake (G3). The SUVmax was measured for each individual tumor. In addition, the intratumoral signal intensity (SI) of the tumor was visually evaluated on T1-weighted TSE, T2-weighted HASTE, and post-contrast VIBE images.

PET/MR mammography

The PET image of the breast was analyzed by using the same method as that of whole-body PET analysis. The findings of DCE-MRI were analyzed with MR BreVis software. For the DCE-MRI analysis, subtraction images were generated by subtracting the pre-contrast images from all contrast-enhanced images. Subsequently, the tumor size, morphologic pattern (shape, margin, and internal enhancement of the mass lesion) during the early phase, and kinetics (percentage SI increase during the early phase and kinetic curve type during the delayed phase) were evaluated for each lesion according to the Breast Imaging Reporting and Data System MRI guidelines [12]. After detection of the enhanced lesions on subtraction images, the region of interest (ROI)-based time–SI curves were plotted at the enhancing tumor to depict enhancement kinetics during the dynamic study. To assess the early-phase SI increase, we calculated the enhancement for the first post-contrast image: percentage enhancement at early phase (%)=[(first post-contrast SI-pre-contrast SI)/pre-contrast SI]×100% [13]. The type of kinetic curve characterized the relative SI change: 3 types of delayed curves were defined: type 1 curve=persistent (continuous increase in SI after peak enhancement >10%); type 2 curve=plateau (steady SI after peak enhancement +/-10%); and type 3 curve=wash out (SI decrease after peak enhancement>10%) [13].

Statistical analysis

The statistical analyses were performed with IBM SPSS statistical software, version 19 (IBM SPSS North America. Chicago, IL, USA). A P value of <0.05 was considered statistically significant. The correlation between $SUV_{whole\text{-}body}$ and $SUV_{mammography}$ was examined using Pearson's correlation and linear regression analysis. We also evaluated the correlation between histologic tumor size and measured tumor size using Pearson's correlation.

Results

Forty-two women, aged 51.8±10.8 years, range, 29-76 years, with 48 IDC (right 23 and left 25) were enrolled in the study. Three patients had multiple IDC. The number of IDC in these 3 patients was 2, 3, and 4, respectively. The average size of the 48 tumors was 1.89±1.19cm (0.2-5.8cm); 10 IDC were ≤1.0cm wide, 24 IDC were 1.1-2.0cm, 13 IDC were 2.1-5.0cm, and 1 IDC was >5.1cm. Furthermore, axillary lymph node metastases were detected in 12 patients.

All patients received surgical treatment within 2 weeks (1-14 days) of the integrated PET/MR examination. Breast-conserving surgery, modified radical mastectomy, and skin-sparing mastectomy were performed in 26, 13, and 3 patients, respectively. Eleven patients received axillary dissection, and 31 patients underwent sentinel lymph node biopsy.

Analysis of whole-body PET/MR

The ^{18}F-FDG avidity of tumors was evaluated by visual analysis

***Table 3**. Lesions characteristics in whole-body PET/MR and PET/MR mammography*

			≤1cm	>1cm	Overall
Number of patients			10	38	48
Tumor size on histology: diameter (mean±SD)			0.65±0.24cm	2.22±1.12cm	1.89±1.19cm
Whole-body PET/MR					
MR	Low SI in T1 TSE		0	25	25
	High SI in HASTE		1	32	33
	Post CM VIBE		4	36	40
PET	Visual analysis	G0	5	0	5
detectability		G1	4	1	5
		G2	0	5	5
		G3	1	32	33
	SUV (mean±SD)		1.2±0.9	4.9±4.8	4.5±4.7
PET/MR mammography					
MR	Enhancement		10	38	48
	Early enhancement (%)		133.4	176.1	167.2
	Delayed enhancement Type				
	Persistent				1
	Plateau		1	0	3
	Washout				43
			2	1	
			6	37	
PET	Visual analysis	G0	5	0	5
	Detectability	G1	4	1	5
	(Same	G2	0	5	5
	as whole-body	G3	1	32	33
	PET/ MR)				
	SUV (mean±SD)		0.7±0.7	3.9±3.9	3.5±3.8

G0: indistinguishable, G1: faint uptake, G2: mild to moderate uptake, G3=distinct uptake,CM: contrast medium; HASTE: half Fourier acquisition single shot turbo spin echo; SI: signal intensity; TSE: turbo spin echo; VIBE: 3-dimensional volumetric interpolated breath-hold examination

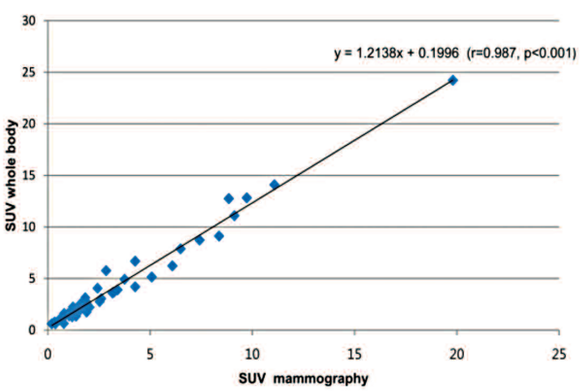

Figure 2. SUV-based evaluation of the correlation of ^{18}F-FDG uptake between whole-body PET/MR and subsequent PET/MR mammography in invasive ductal carcinoma. The x-axis displays quantitative values obtained by PET/MR mammography, and the y-axis displays the corresponding values obtained by whole-body PET/MR.

and semiquantitative analysis with SUV. There were 10 IDC with no or very weak uptake (G0 or G1), 5 G2, and 33 G3. According to the size of the tumor, we classified IDC into 2 groups: 1.0cm or smaller, Group A and larger than 1.0cm, Group B. Group A tumors were further classified as follows: G0, 5; G1, 4; and G3, 1. Group B tumors were classified as follows: G1, 1; G2, 5; and G3, 32. Excluding G0, the mean SUV was 1.2±0.9 in Group A, 4.9±4.8 in Group B, and 4.5±4.7 overall.

More than half: 25/48 of IDC showed low SI by T1-weighted TSE, and more than two thirds, 33/48 showed high SI by T2-weighted fs HASTE. In the post-contrast VIBE images, even more, 40/48 IDC showed enhancement. In Group A, the T1-weighted TSE image did not show any lesion with low SI; there was 1 (10%) high SI mass observed by T2-weighted fs HASTE and 4 enhancing masses (40%) observed by VIBE. In Group B, two thirds, 25/48 IDC showed low SI lesions on T1-weighted TSE images, more, 32/48 showed high SI lesions on T2-weighted fs HASTE images, and even more, (94.7%) 36/48 showed enhancing masses on VIBE images (Table 3).

Analysis of PET/MR mammography

No difference in ^{18}F-FDG uptake was observed between whole-body PET/MR and PET/MR mammography. Excluding G0, the mean SUV was 0.7±0.7 in Group A, 3.9±3.9 in Group B, and 3.5±3.8 overall. A strong and highly significant correlation was found between $SUV_{whole\ body}$ and $SUV_{mammography}$ ($r=0.987$, $P<0.001$; Fig. 2).

All IDC showed contrast enhancement in DCE-MRI findings. The size of the tumor measured by PET/MR mammography was 2.0±1.2cm, which was closely related to the size measured by histological analysis ($r=0.925$, $P<0.001$).

Furthermore, the IDC were observed to have the following morphologies: 4 IDC, round; 6, oval; 18, lobular; 20, irregular; 22, spiculated; 10, smooth margin; 22, irregular margin; and 16, spiculated margin. Analysis of the internal enhancement

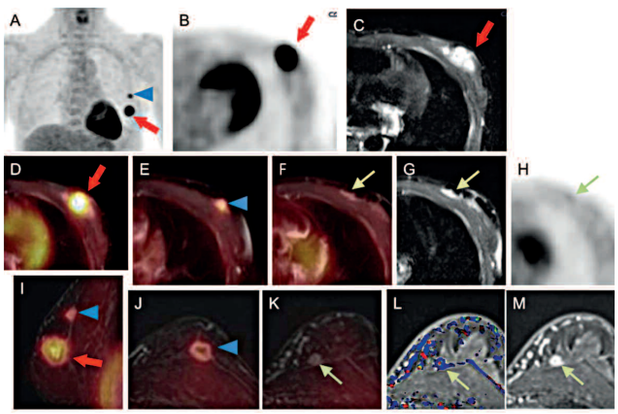

Figure 3. A 52 years old woman with 3 invasive ductal carcinomas (thick arrow: 2cm-wide mass in the 11′ direction; arrowhead: 1.1cm-wide mass in the 12′ direction; thin arrow: 0.8cm-wide mass in the 11′ direction) in her left breast. She underwent PET/MR examination for preoperative evaluation.
(A) Maximum-intensity projection image of ^{18}F-FDG PET shows only 2 hypermetabolic masses (thick arrow and arrowhead) in the left breast. (B) Axial MR attenuation-corrected PET image shows a hypermetabolic lesion in the left 11′ direction (thick arrow). (C) Axial T2 HASTE fs image shows high SI lesion in the left 11′ direction (thick arrow). (D, E, and F) Axial PET/MR images show high ^{18}F-FDG uptake (SUVmax 6.68) in the left 11′ direction, focal ^{18}F-FDG uptake (SUVmax 3.14) in the left 12′ direction, and suspicious ^{18}F-FDG uptake in the left 11′ direction. (G) Axial T2 HASTE fs image shows high SI lesion in the left 11′ direction. (H) Axial PET image shows suspicious increased ^{18}F-FDG uptake lesion in the left 11′ direction. (I) Sagittal image of PET/MR mammography shows excellent spatial and geometric overlap of the breast lesions of ^{18}F-FDG uptake. (J and K) Axial PET/MR mammography show excellent spatial and geometric overlap of the breast lesions with moderate ^{18}F-FDG uptake in 12′ and faint ^{18}F-FDG uptake in 11′ directions, depicting good enhancement, respectively. (L and M) DCE MRI shows a well-enhancing mass with rapid increase and washout kinetics in the 11′ direction.

pattern of the IDC revealed the following patterns: homogeneous, 8; heterogeneous, 31; rim enhancement, 8; and central enhancement, 1. The mean of the initial peak was 167.2±62.7%, including 1 tumor showing slow increase during the early phase. During the delayed phase, 43 IDC showed washout kinetics, 3 showed a plateau, and only 1 showed a persistent type.

Discussion

In this study, we investigated the use of hybrid imaging in patients with IDC and found that PET/MR mammography was feasible and more useful than whole-body PET/MR imaging in the diagnosis of IDC.

Only one of the ten ≤1cm wide tumors showed increased ^{18}F-FDG uptake. We could detect 5/10 tumors by whole-body PET/MR images, considering both ^{18}F-FDG PET and anatomical changes revealed by MRI. However, PET/MR mammography showed all 10 tumors with contrast enhancement. Thus, whole-body PET/MR was not sufficient for the diagnosis of breast malignancy, whereas PET/MR mammography could detect small lesions in addition to possible multiple tumors [14] (Fig. 3).

The average size of the tumors included in this study was <2cm; therefore, conventional whole-body PET/MR could not detect these tumors during the diagnosis of breast cancer. On the other hand, PET/MR mammography could depict the shape, margin, and internal enhancement pattern of these tumors; it could also show the enhancement pattern over time as well as the ^{18}F-FDG avidity. Therefore, PET/MR mammography is more suitable than whole-body PET/MR imaging for the morphologic evaluation of tumors larger than 1cm in size as well as for the detection of small lesions. Features such as the shape, margin, and internal enhancement patterns are also useful tools for distinguishing malignant from benign lesions [15]. We did not include benign disease in this study, and therefore, we could not evaluate the differential diagnosis of malignant and benign lesions by PET/MR mammography. However, it is likely that the metabolic and morphologic information obtained by PET/MR mammography can increase the diagnostic accuracy of malignant tumors. Moy et al [16] reported that fused PET/MR mammography could increase the positive predictive value and specificity compared to MR imaging alone and the sensitivity and negative predictive value compared to ^{18}F-FDG PET alone.

No difference in ^{18}F-FDG uptake between whole-body PET/MR and PET/MR mammography was observed. The correlation between $SUV_{whole\ body}$ and $SUV_{mammography}$ was strong and highly significant. However, a steady percentage of radioactivity attenuation was observed due to radiofrequency of the breast coil. In the near future, commercialization of the radiofrequency breast coil may result in the development of breast coils with no global attenuation on the PET emission data; in addition, further improvement of the resolution of the PET detector is expected.

Positron emission tomography imaging with the patient in the prone position is more useful than that in the supine position for detecting lesions and understanding anatomical locations because it is more representative of the original anatomy that relies on gravity. Besides, it is favorable for the co-registration of PET data and MR anatomical information.

Recently, positron emission mammography (PEM) was developed and applied in clinical practice. Positron emission mammography uses a dedicated scanner for breast cancer detection with 2 parallel photon detectors similar to mammography compressors [17]. Positron emission mammography was more sensitive than whole-body PET/CT in evaluating breast cancer, with a high sensitivity for tumors smaller than 1cm [18]. Moreover, the sensitivity, specificity, and diagnostic capability of PEM were higher than those of MRI [19]. If the sensitivity of the PET detector in the PET/MR scanner could be similar to that of PEM, PET/MR mammography could be used to detect smaller lesions with low ^{18}F-FDG avidity and provide more detailed molecular information in small-sized breast cancer.

To take advantage of the unique features of the integrated PET/MR scanner, it is important to use MRI not only for anatomical reference using PET images but also for assessing the detailed architecture and obtaining functional information by using novel MRI techniques. The aforementioned uses of PET/MR differentiate it from PET/CT, in which low-dose CT data are used for anatomical reference and attenuation correction. Although diffusion-weighted imaging (DWI) was not performed in this study, a recent study showed a significant negative correlation between standardized uptake value (SUV) and the apparent diffusion coeffi-

cient (ADC) [20]. In addition, the SUV and ADC values were correlated to several histopathological prognostic factors, which contribute to the prognosis of breast cancer [20-22]. The information provided by both PET and DWI can be complementary because the 2 modalities provide different biophysical and biochemical information. It is expected to be useful in predicting the prognosis and evaluating the therapeutic effect in multi-parametric quantitative analysis using ^{18}F-FDG avidity, DWI, and DCE, etc.

Our study has several limitations. First, the number of subjects was small. Second, we did not include patients with benign disease because the PET/MR study was performed for staging of breast cancer before the operation. If PET/MR mammography were used for the differential diagnosis of malignant and benign masses, it would increase the specificity, similar to that of PEM. Third, the breast coil used in this study was not an approved surface coil; therefore, it resulted in global attenuation on the PET emission data. However, the correlation between SUV of whole-body PET/MR and that of PET/MR mammography was very good. Therefore, attenuation induced by the radiofrequency of the breast coil may not be an obstacle in the clinical use of PET/MR mammography. Moreover, in the near future, the following technological developments will further improve this technique-software for high resolution reconstruction, an advanced detector such as Silicon Photomultiplier (SiPM), and approved surface coils for PET/MR mammography that consider attenuation. These developments could make PET/MR mammography more useful in diagnosis and prognostic estimation by improving the signal-to noise ratio [23].

The small number of subjects in this study was not enough to show the additional advantages of integrated PET/MR mammography because both PET and MRI are good individual diagnostic modalities for breast cancer. Nevertheless, PET/MR mammography was shown to be useful for the diagnosis of small lesions; it revealed metabolic characteristics that make it an excellent imaging technique. Importantly, this integrated PET/MR study for the diagnosis of breast cancer is the first of its kind. This is the first study in integrated PET/MR system with simultaneous PET and MR acquisition. Previous studies [20-22] were not performed in the integrated system. They were performed in separated PET/CT and MRI at different times. Further investigations, which involve diverse histologic types of breast cancer and predict prognosis and therapeutic responses by using PET/MR mammography, must be performed to establish the use of this hybrid technique for the diagnosis of breast cancer.

In conclusion, the combined use of whole-body PET/MR and PET/MR mammography demonstrated the potential of a "one-stop shop" modality for the preoperative evaluation of breast cancer. PET/MR mammography might especially be useful in the detection of small lesions with no ^{18}F-FDG uptake, may provide more detailed anatomic information and help in tumor characterization of ^{18}F-FDG-avid lesions.

Acknowledgement

This research was supported by Yeungnam University research grants (2011).

The authors declare that they have no conflicts of interest.

Bibliography

1. Kjaer A, Loft A, Law I et al. PET/MRI in cancer patients: first experiences and vision from Copenhagen. *MAGMA* 2013; 26: 37-47.
2. Drzezga A, Souvatzoglou M, Eiber M et al. First clinical experience with integrated whole-body PET/MR: comparison to PET/CT in patients with oncologic diagnoses. *J Nucl Med* 2012; 53: 845-55.
3. Wetter A, Lipponer C, Nensa F et al. Evaluation of the PET component of simultaneous [^{18}F]choline PET/MRI in prostate cancer: comparison with [^{18}F]choline PET/CT. *Eur J Nucl Med Mol Imaging* 2014; 41: 79-88.
4. Weir L, Worsley D, Bernstein V. The value of FDG positron emission tomography in the management of patients with breast cancer. *Breast J* 2005; 11: 204-9.
5. Eubank WB, Mankoff DA. Evolving role of positron emission tomography in breast cancer imaging. *Semin Nucl Med* 2005; 35: 84-99.
6. Lind P, Igerc I, Beyer T et al. Advantages and limitations of FDG PET in the follow-up of breast cancer. *Eur J Nucl Med Mol Imaging* 2004; 31 (Suppl 1): S125-34.
7. Czernin J. FDG-PET in breast cancer: a different view of its clinical usefulness. *Mol Imaging Biol* 2002; 4: 35-45.
8. Avril N, Rose CA, Schelling M et al. Breast imaging with positron emission tomography and fluorine-18 fluorodeoxyglucose: use and limitations. *J Clin Oncol* 2000; 18: 3495-502.
9. Kumar R, Chauhan A, Zhuang H et al. Clinicopathologic factors associated with false negative FDG-PET in primary breast cancer. *Breast Cancer Res Treat* 2006; 98: 267-74.
10. Martinez-Moller A, Souvatzoglou M, Delso G et al. Tissue classification as a potential approach for attenuation correction in whole-body PET/MRI: evaluation with PET/CT data. *J Nucl Med* 2009; 50: 520-6.
11. Martinez-Moller A, Eiber M, Nekolla SG et al. Workflow and scan protocol considerations for integrated whole-body PET/MRI in oncology. *J Nucl Med* 2012; 53: 1415-26.
12. American College of Radiology. *Breast imaging reporting and data system: breast imaging atlas (BI-RADS)*. 4th edn. Reston Va: Amer Coll Radiol; 2003: 1-114.
13. Kuhl CK, Mielcareck P, Klaschik S et al. Dynamic breast MR imaging: are signal intensity time course data useful for differential diagnosis of enhancing lesions? *Radiology* 1999; 211: 101-10.
14. Drew PJ, Chatterjee S, Turnbull LW et al. Dynamic contrast enhanced magnetic resonance imaging of the breast is superior to triple assessment for the pre-operative detection of multifocal breast cancer. *Ann Surg Oncol* 1999; 6: 599-603.
15. Szabo BK, Aspelin P, Wiberg MK, Bone B. Dynamic MR imaging of the breast. Analysis of kinetic and morphologic diagnostic criteria. *Acta Radiol* 2003; 44: 379-86.
16. Moy L, Noz ME, Maguire GQ, Jr. et al. Role of fusion of prone FDG-PET and magnetic resonance imaging of the breasts in the evaluation of breast cancer. *Breast J* 2010; 16: 369-76.
17. MacDonald L, Edwards J, Lewellen T et al. Clinical imaging characteristics of the positron emission mammography camera: PEM Flex Solo II. *J Nucl Med* 2009; 50: 1666-75.
18. Kalinyak JE, Berg WA, Schilling K et al. Breast cancer detection using high-resolution breast PET compared to whole-body PET or PET/CT. *Eur J Nucl Med Mol Imaging* 2014; 41(2): 260-75.
19. Narayanan D, Madsen KS, Kalinyak JE, Berg WA. Interpretation of positron emission mammography and MRI by experienced breast imaging radiologists: performance and observer reproducibility. *Am J Roentgenol* 2011; 196: 971-81.
20. Nakajo M, Kajiya Y, Kaneko T et al. FDG PET/CT and diffusion-weighted imaging for breast cancer: prognostic value of maximum standardized uptake values and apparent diffusion coefficient values of the primary lesion. *Eur J Nucl Med Mol Imaging* 2010; 37: 2011-20.
21. Ueda S, Tsuda H, Asakawa H et al. Clinicopathological and prognostic relevance of uptake level using ^{18}F-fluorodeoxyglucose positron emission tomography/computed tomography fusion imaging (^{18}F-FDG PET/CT) in primary breast cancer. *Jpn J Clin Oncol* 2008; 38: 250-8.
22. Choi BB, Kim SH, Kang BJ et al. Diffusion-weighted imaging and FDG PET/CT: predicting the prognoses with apparent diffusion co efficient values and maximum standardized uptake values in patients with invasive ductal carcinoma. *World J Surg Oncol* 2012; 10: 126.
23. Yoon HS, Ko GB, Kwon SI et al. Initial results of simultaneous PET/MRI experiments with an MRI-compatible silicon photomultiplier PET scanner. *J Nucl Med* 2012; 53: 608-14.